

## Short-range magnetic collapse of Fe under high pressure at high temperatures observed using x-ray emission spectroscopy

J.-P. Rueff,<sup>1,2,\*</sup> M. Mezouar,<sup>3</sup> and M. Acet<sup>4</sup>

<sup>1</sup>Synchrotron SOLEIL, L'Orme des Merisiers, Saint-Aubin, Boîte Postale 48, 91192 Gif-sur-Yvette Cedex, France

<sup>2</sup>Laboratoire de Chimie Physique-Matière et Rayonnement (UMR 7614), Université Pierre et Marie Curie, 11 rue Pierre et Marie Curie, 75231 Paris Cedex 05, France

<sup>3</sup>ESRF, 6 rue Jules Horowitz, Boîte Postale 220, 38043 Grenoble Cedex, France

<sup>4</sup>Experimentalphysik, Universität Duisburg-Essen, D-47048 Duisburg, Germany

(Received 1 September 2008; published 29 September 2008)

Understanding the high-pressure electronic properties of Fe still poses both theoretical and experimental challenges. Here, we evidence the short-range magnetic collapse of Fe in the  $\gamma$  phase by x-ray emission spectroscopy carried out *in situ* under high-pressure and high-temperature conditions, up to 20 GPa and 1400 K. We find an abrupt decrease in the Fe spin state in  $\gamma$ -Fe at high pressure similar in amplitude to the known  $\alpha$ - $\varepsilon$  magnetic collapse transition. A careful analysis of the Fe spin state in the  $\varepsilon$  phase indicates a sluggish diminution right above the transition pressure, bearing out recent predictions of residual, likely noncollinear, magnetism in this phase. In the  $\gamma$  phase, our results demonstrate that the dominant mechanism at high pressure is a high-spin to low-spin transition. Implications for the elastic properties of Fe at extreme conditions are analyzed.

DOI: 10.1103/PhysRevB.78.100405

PACS number(s): 78.70.En, 71.20.Eh, 71.27.+a

Fe is the constant, yet not exhausted, subject of studies aiming at revealing its properties under high-pressure (HP) and high-temperature (HT) conditions. The knowledge of the Fe phase diagram is not only of importance for geophysics and geodynamics, Fe being the most abundant element of the earth interior, but also serves as a model system for the theoretical understanding of 3d electronic properties. High-pressure magnetism more particularly is believed to play a crucial role in the stability of the Fe structural phases and elastic properties. Theoretical improvements beyond the local-density approximation make it now possible to derive the correct Fe magnetic ground state at ambient conditions. However, puzzling results recently observed in Fe under extreme conditions have spun the situation anew. Among these, the superconductivity found in Fe along with ferromagnetism at low temperature and HP (Ref. 1) and the anomalous splitting of Raman spectra<sup>2</sup> in  $\varepsilon$ -Fe, the nonmagnetic hcp HP phase, reportedly due to antiferromagnetic coupling.<sup>3</sup> Even more poorly understood is the  $\gamma$ -Fe fcc phase stabilized at HT and HP. First-principles calculations favor a noncollinear magnetism,<sup>4-11</sup> but results in the  $\gamma$  phase are extremely scarce because of the HP/HT experimental constraints. Here, we report on the collapse of the short-range iron magnetic state in the HP/HT phases by x-ray emission spectroscopy (XES), a local probe of the 3d spin magnetic moment.

In the  $\gamma$  phase, Fe supposedly adopts a spin spiral density wave (SSDW) with a propagation vector  $\mathbf{q}=(0, k, 1)\frac{2\pi}{a}$  along the  $XW$  direction of the Brillouin zone, with  $k\sim 0.1$  (Ref. 12) close to that of a type-I antiferromagnetic system. This value was derived from early neutron measurements of  $\gamma$ -Fe precipitates contained in a Cu matrix, while the SSDW structure was confirmed by first-principles calculations.<sup>4-11</sup> In general, these give a stable energy minimum for wave vector  $\mathbf{q}=(0, 0, 0.6)\frac{2\pi}{a}$  along the  $\Gamma X$  direction at high volume and solutions closer to the  $X$  point at low volume. But, as it turns out, there is no direct investigation reported so far of the Fe

magnetic properties in the  $\gamma$  phase under *in situ* HP/HT conditions against which the calculations can be tested. One might especially question the validity of the long-range magnetic structures calculated at  $T=0$  K as a realistic starting point to describe the high-pressure  $\gamma$ -Fe properties. Additionally, the supposed anti-Invar character of  $\gamma$ -Fe (Ref. 13) entails a coupling to the local spin state. This is likely to occur at extreme conditions in the form of a magnetovolume instability, which needs to be accounted for. Providing clear-cut evidence of such instability, however, requires it to be away from any long-range magnetic ordering (which causes a decrease in Curie temperature) and applied pressure.

To that aim, we have performed a combined spectroscopic and structural investigation of Fe in the  $\alpha$ ,  $\varepsilon$ , and  $\gamma$  phases under HP HT conditions. The x-ray diffraction (XRD) and x-ray emission spectra were measured on ID-27 at the European Synchrotron Radiation Facility (ESRF). The incident beam is monochromatized by double reflection on cryogenically cooled Si(111) crystals and focused at the sample position in  $4\times 8\ \mu\text{m}^2$  spot by a pair of Kirkpatrick-Baez (KB) mirrors. The sample, a high-purity 15- $\mu\text{m}$ -thick Fe foil, was loaded in a diamond anvil cell. We used 300  $\mu\text{m}$  culet diamonds and a 40- $\mu\text{m}$ -thick rhenium gasket. The sample was thermally isolated from the diamonds on both sides by a sandwich of compacted  $\text{Al}_2\text{O}_3$  powder also serving as a pressure transmitting medium. High-temperature XES measurements were realized by double-sided laser heating technique, following the pioneer work of Lin *et al.*<sup>14</sup> The setup installed on the ID-27 beamline is described elsewhere.<sup>15</sup> It includes a Nd-doped yttrium aluminum garnet laser with focusing optics to produce a large and homogeneous heated area and collecting mirrors for *in situ* temperature measurements. Thus, temperature gradients are avoided to a large extent (less than 2%) as the x-ray spot is about five times smaller than the laser spot. Temperature was estimated by spectroradiographic method using Schwarzschild optics while pressure

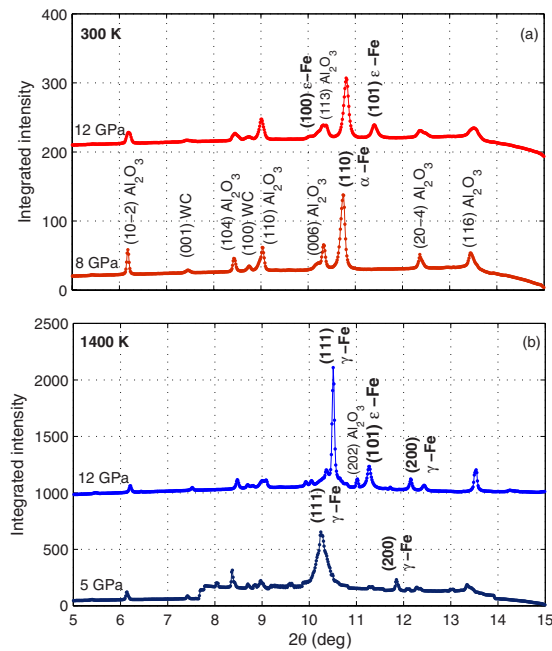


FIG. 1. (Color online) X-ray powder-diffraction patterns of Fe at ambient (panel *a*) and high temperature (panel *b*) in the  $\alpha$  and  $\gamma$  phase, respectively.

calibration was based on the ruby fluorescence technique. The XRD pattern was recorded by angular dispersive method on a MARCCD 165 detector at a fixed wavelength of 0.3738 Å. The corresponding energy (33.168 keV) is larger than the 1s-Fe ionization threshold permitting the simultaneous measurements of the XES  $K\beta$  fluorescence. The emission spectra were acquired by a 1-m radius spectrometer placed on the optics table. The spectrometer was equipped with a Si(531) spherically bent analyzer and a solid state detector laid in the Rowland circle geometry. Since the x-ray spot coincides exactly with the laser beam and the focal point of the Schwarzschild optics, it is always possible to associate with a given XES spectrum the right structural phase and temperature without any possible confusion.

Figure 1 shows the XRD pattern measured at 300 K and 1400 K for low and high pressures. As the laser beam is very local, heating can be turned on and off fast and in a reliable manner. The data confirm the stabilization of  $\alpha$ -Fe at low  $T$  and  $\gamma$ -Fe at high  $T$  in addition to a weak contribution from the nonmagnetic  $\varepsilon$ -Fe phase, which emerges in the high-pressure region. The other diffraction peaks can be associated to the pressure medium and tungsten carbide diamonds seats as shown in Fig. 1. The lattice parameters summarized in Table I for the different phases are consistent with the reported values.<sup>16</sup>

The local magnetic state of iron was probed by XES at the Fe  $K\beta$  ( $3p \rightarrow 1s$ ) line. The  $K\beta$  cross section is proportional to  $|\langle 1s3d^m | T_1 | 3p3d^m \rangle|^2 \delta(E_f - E_i - \hbar\omega)$ , where  $T_1$  is the dipolar operator,  $\hbar\omega$  the emitted photon energy, and  $E_f(E_i)$  the final (initial) state energy. The sensitivity to 3d magnetism arises from the 3p-3d exchange interaction in the XES final state, which splits the spectrum into principally a main peak and a low-energy satellite. These features originate from the two possible orientations of the 3p core-hole spin with respect to

TABLE I. Lattice parameters in Å for the different phases of Fe observed at 300 and 1400 K.

300 K	8 GPa	12 GPa
$\alpha$ -Fe: $a$	2.825 Å	2.805 Å
$\varepsilon$ -Fe: $a(c)$		2.47(3.94) Å
1400 K	5 GPa	12 GPa
$\gamma$ -Fe: $a$	3.620 Å	3.535 Å
$\varepsilon$ -Fe: $a(c)$		2.505(3.975) Å

the 3d majority-spin. When the 3d spin state is modified so are the intensity ratio and energy splitting of the two features.<sup>17,18</sup> The pressure dependence of the XES spectra is presented in Fig. 2 for both  $\alpha$ -Fe(300 K) and  $\gamma$ -Fe(1400 K) states. The former set has been already measured<sup>19</sup> and can serve to validate the new HT/HP XES setup at ID-27, whereas the *in situ* measurements of the Fe magnetic state in the  $\gamma$  phase are new. In Fe metal, the satellite is notably weaker than that in the Fe oxides.<sup>20,21</sup> We clearly notice, nevertheless, a decrease in the satellite intensity at high pressure, which suggests a change in the Fe spin state. The magnetic information contained in the XES spectra is not readily usable in the absence of formal sum rules but can be extracted accurately, albeit on a relative scale, by means of integrated differences. The phenomenological method developed in Ref. 19 has been successively tested in a large series of transition-metal compounds (cf. Refs. 22–24). We have followed the procedure described in Ref. 25 to extract the integrated absolute difference (IAD), a quantity that is linearly related to the spin magnetic moment of the Fe atoms. It is derived from the absolute value of the difference spectrum between a given pressure  $P$  and the zero pressure  $P_0$ , integrated over the entire  $K\beta$  spectral range in a 50 eV window:  $IAD(P) = \int |I_{XES}(P, \omega) - I_{XES}(P_0, \omega)| d\omega$ , with  $I_{XES}$  as the  $K\beta$  normalized intensity.

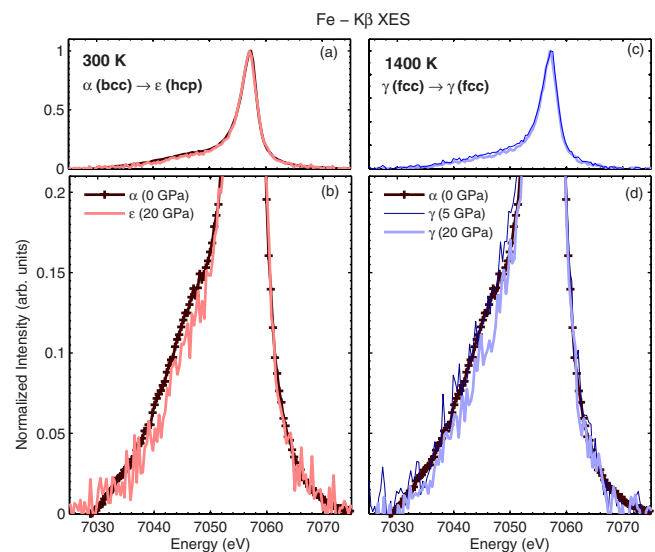


FIG. 2. (Color online) XES spectra of the Fe  $K\beta$  emission line in Fe measured under high-pressure and temperature conditions in the  $\alpha$ - $\varepsilon$  (panel *a*) and  $\gamma$  phases (panel *c*). The spectra are shown on an expanded scale in panels *b* and *d*, respectively.

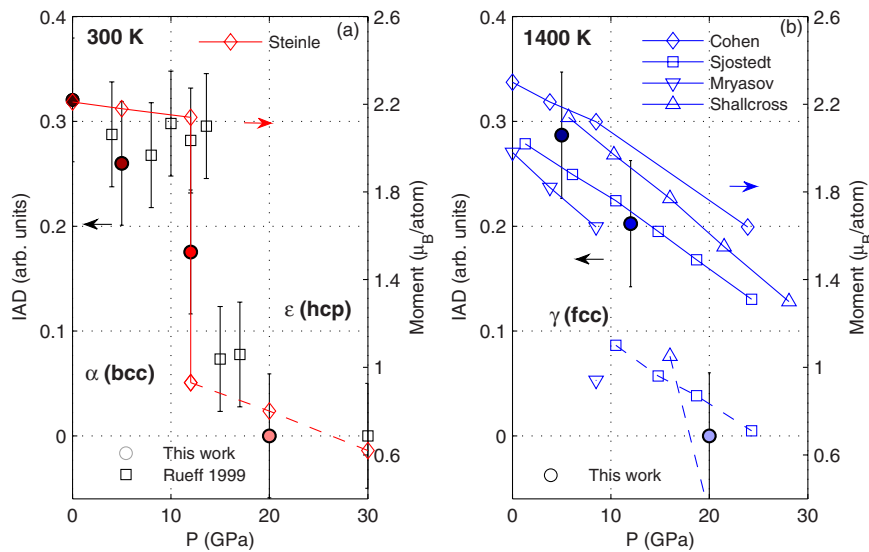


Figure 3 shows the pressure dependence of the Fe spin state from the IAD analysis. The results at 300 K in the  $\alpha$  phase agree well with our previous measurements that we have carefully reanalyzed along the same lines, although the number of pressure points is fairly reduced in the present data set. As previously reported by different techniques including XES and Mössbauer spectroscopy,<sup>26</sup> the data bear out the strong reduction in the spin state when Fe enters the  $\epsilon$  phase at high pressure. Additionally, we observe here a nonvanishing magnetism above the transition that decays at higher pressure. This can be compared to recent first-principles calculations of the magnetic moment of iron as a function of pressure in  $\epsilon$ -Fe allowing for noncollinearity,<sup>3</sup> and in Fig. 3(a), the calculations (right scale) are compared to the experimental data (left scale). In contrast to the high-spin (HS) to low-spin (LS) transition usually evoked at the  $\alpha$ - $\epsilon$  structural change, the authors in Ref. 3 argue that the Fe magnetic moment is not completely suppressed in  $\epsilon$ -Fe but instead remains up to a fairly large pressure in presence of type-II antiferromagnetic coupling. This would explain why Mössbauer spectroscopy consistently finds the disappearance of magnetism at the  $\alpha$ - $\epsilon$  transition pressure since the hyperfine splitting is significantly reduced in the  $\epsilon$  phase—in fact well below the detection limit—while XES provides a non-zero magnetic moment right above the transition. At higher pressure above the structural transition, the magnetic moment is predicted to slowly decrease up to 50 GPa in fair agreement with the experimental spin state derived from XES up to 30 GPa.

The behavior in  $\gamma$ -Fe shows remarkable resemblance with the modification of the Fe magnetism in the  $\alpha$  phase under pressure. The IAD analysis reported in Fig. 3(b) indicates a decrease in the magnetic moment with pressure of similar amplitude. This suggests that besides the occurrence of the SSDW, the mechanism of the magnetic transition in the  $\gamma$  phase primarily involves a high-spin to low-spin transition. As further evidence, we show on the right scale in Fig. 3(b) the theoretical magnetic moment of Fe computed from first-principles calculations as found in recent literature (see legend for details). We used the equation of state of Ref. 28 to convert the computed volume to pressure. At this point, two

FIG. 3. (Color online) (Left scale) IAD derived from Fig. 2 (filled circles); (right scale) spin state obtained from comparison with theoretical calculations from Ref. 27 in the  $\epsilon$  phase (panel a) and Refs. 4, 8, 10, and 11 in the  $\gamma$  phase (panel b) (open symbols). Solid (dashed) lines indicate high-spin (low-spin) states.

different aspects have to be considered: the  $q$  dependence of the Fe local magnetic moment  $m(q)$  and the stabilization of the low-spin configuration at low volume. The top curves in Fig. 3(b) show the calculated values of  $m(q)$  at  $q \sim 0.6$ , which minimizes the total energy of the system. We find a fair agreement at low pressure between the XES extracted values and the calculated moments for all the data sets, but at high pressure the measured Fe magnetic moment is significantly lower than the ones calculated at this  $q$  value. A better agreement is found by considering  $\lim_{q \rightarrow 0} m(q)$  in the high-pressure region [bottom curves in Fig. 3(b)]. The low  $q$  limit of the SSDW corresponds to a magnetic state with saturated ferromagnetism and a clearly defined HS-to-LS transition. Uncertainty is large both in the experimental spin state at high pressure and in the choice of the  $q$  value for the calculated magnetic moment. The results nevertheless suggest that at high pressure  $\gamma$ -Fe is in the LS state and adopts a more collinear (if not a ferromagnetic) structure than usually considered, in agreement with neutron diffraction that demon-

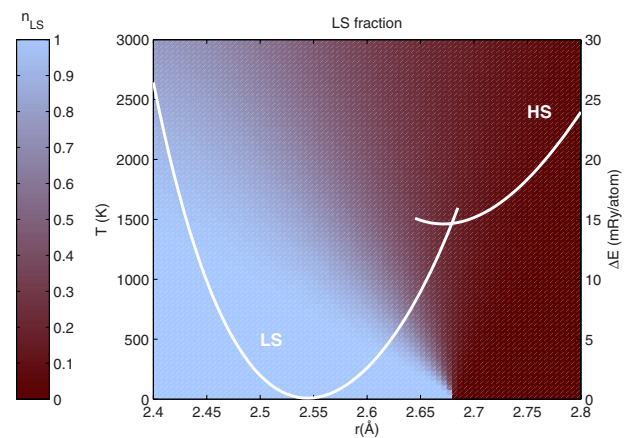


FIG. 4. (Color online) Spin state of  $\gamma$ -Fe as function of temperature (left scale) and atomic volume (bottom scale). The solid curves taken from Ref. 30 indicate the total energy of the HS and LS states (right scale). The amount of LS spin state  $n_{LS}$  computed from these values is shown on a color scale, from light (full LS) to dark (full HS).

strates only FM short-range correlations in  $\gamma$ -like Fe.<sup>29</sup> This minimizes substantially the role of SSDW in the magnetic change at extreme conditions in the  $\gamma$  phase.

The large decrease in the local spin state in the  $\gamma$  phase impacts not only magnetism as just discussed but also the elastic properties of HP/HT Fe. The magnetoelastic effects can be understood through the total energy analysis such as in the fixed-spin-moment method; the case of fcc Fe was more explicitly discussed in Refs. 30 and 31. The authors considered an assembly of HS, LS, or nonmagnetic (NM) ions with FM or AF magnetic arrangements. In  $\gamma$ -Fe, the FM state (HS) is found at slightly higher energies (several meV) than the NM or AF state (LS). The stable state at  $T=0$  K is the AF state while the FM state is stabilized above a critical volume larger than the equilibrium volume where the AF and FM branches cross. The FM stability range can be reached by applying a negative pressure or increasing  $T$ , which is indeed the case here. At high pressure, the system is forced

back to the low volume, LS region that is energetically favorable.

Thus, similar to Invar, where the LS state is stabilized at high pressure, the magnetic collapse observed in  $\gamma$ -Fe can be correlated with a magnetovolume instability. To illustrate this behavior, we have computed in Fig. 4 the spin state fraction ( $n_{LS}$ ) from the total energy difference  $\Delta E$  borrowed from Ref. 30. In a Boltzmann statistics approach,  $n_{LS}=[1+g_{HS}/g_{LS}\exp(-\beta\Delta E)]^{-1}$ , where  $\beta=k_B T$  and  $g_{(LS,HS)}$  is the degeneracy. Consistent with the picture provided by XES, the HS-high-volume state is found to be stable on the low-pressure and high- $T$  side while the LS-low-volume state is stabilized at HP and low  $T$ . That the LS configurations are stabilized under pressure both at low ( $\epsilon$ -Fe) and high  $T$  ( $\gamma$ -Fe) will affect the general structural stability of Fe at extreme conditions.

We thank R. Cohen for useful discussions about the SSDW state in  $\gamma$ -Fe.

\*jean-pascal.rueff@synchrotron-soleil.fr

<sup>1</sup>K. Shimizu *et al.*, Nature (London) **412**, 316 (2001).

<sup>2</sup>S. Merkel *et al.*, Science **288**, 1626 (2000).

<sup>3</sup>G. Steinle-Neumann *et al.*, Proc. Natl. Acad. Sci. U.S.A. **101**, 33 (2004).

<sup>4</sup>O. N. Mryasov *et al.*, Phys. Rev. B **45**, 12330 (1992).

<sup>5</sup>K. Hirai, J. Phys. Soc. Jpn. **61**, 2491 (1992).

<sup>6</sup>L. Stixrude *et al.*, Phys. Rev. B **50**, 6442 (1994).

<sup>7</sup>P. Söderlind *et al.*, Phys. Rev. B **53**, 14063 (1996).

<sup>8</sup>E. Sjöstedt and L. Nordström, Phys. Rev. B **66**, 014447 (2002).

<sup>9</sup>Y. Kakehashi *et al.*, Phys. Rev. B **65**, 134418 (2002).

<sup>10</sup>R. E. Cohen and S. Mukherjee, Phys. Earth Planet. Inter. **143-144**, 445 (2004).

<sup>11</sup>S. Shallcross *et al.*, Phys. Rev. B **73**, 104443 (2006).

<sup>12</sup>Y. Tsunoda, J. Phys.: Condens. Matter **1**, 10427 (1989).

<sup>13</sup>M. Acet *et al.*, Phys. Rev. B **49**, 6012 (1994).

<sup>14</sup>J.-F. Lin *et al.*, J. Synchrotron Radiat. **12**, 637 (2005).

<sup>15</sup>E. Schultz *et al.*, High Press. Res. **25**, 71 (2005).

<sup>16</sup>W. Pepperhoff and M. Acet, *Constitution and Magnetism of Iron*

*and its Alloys* (Springer, Heidelberg, 2001), Vol. 8.

<sup>17</sup>F. M. F. de Groot *et al.*, J. Phys.: Condens. Matter **6**, 6875 (1994).

<sup>18</sup>X. Wang *et al.*, Phys. Rev. B **56**, 4553 (1997).

<sup>19</sup>J.-P. Rueff *et al.*, Phys. Rev. B **60**, 14510 (1999).

<sup>20</sup>J. Badro *et al.*, Science **305**, 383 (2004).

<sup>21</sup>A. Mattila *et al.*, Phys. Rev. Lett. **98**, 196404 (2007).

<sup>22</sup>G. Vankó *et al.*, Phys. Rev. B **73**, 024424 (2006).

<sup>23</sup>R. Lengsdorf *et al.*, Phys. Rev. B **75**, 180401(R) (2007).

<sup>24</sup>J.-F. Lin *et al.*, Science **317**, 1740 (2007).

<sup>25</sup>G. Vankó *et al.*, J. Phys. Chem. B **110**, 11647 (2006).

<sup>26</sup>R. Taylor *et al.*, J. Appl. Phys. **69**, 6126 (1991).

<sup>27</sup>G. Steinle-Neumann *et al.*, J. Phys.: Condens. Matter **16**, S1109 (2004).

<sup>28</sup>R. Boehler *et al.*, J. Appl. Phys. **65**, 1795 (1989).

<sup>29</sup>M. Acet *et al.*, Europhys. Lett. **40**, 93 (1997).

<sup>30</sup>V. L. Moruzzi *et al.*, Phys. Rev. B **34**, 1784 (1986).

<sup>31</sup>V. L. Moruzzi *et al.*, Phys. Rev. B **39**, 6957 (1989).